

Observation from space of meteorological fields at the scale of regional Numerical Weather Forecast models^(*)

G. PERONA⁽¹⁾, R. NOTARPIETRO⁽¹⁾, M. GABELLA⁽¹⁾ and A. SPERANZA⁽²⁾

⁽¹⁾ *Dipartimento di Elettronica, Politecnico di Torino - C.so Duca degli Abruzzi 24
10129 Torino, Italy*

⁽²⁾ *Dipartimento di Matematica e Fisica, Università di Camerino - Via del Bastione 3
62032 Camerino (MC), Italy*

(ricevuto il 19 Settembre 2002; revisionato il 24 Novembre 2003; approvato il 18 Dicembre 2003)

Summary. — In this paper we report the results of feasibility studies concerning the use of radars on polar orbiting space-platforms for the direct observation of meteorological fields (in particular large-scale vertical velocity) that are crucial in the initialisation and verification of models for NWF (Numerical Weather Forecast). Specifically, we have made reference to LAM (Limited Area Models) with horizontal grid-size of the order of 10 km that is typical of models currently used for service operations at regional scale. The original motivation of the research reported in this paper was to study the possibility of using the “Cassini radar” from the International Space Station (ISS), having as observational target the sub-synoptic features connected with intense precipitation in the Mediterranean area. Possible generalizations to other instruments (in particular, a clear-air satellite-based radar) and other phenomenologies (rain fields) have been considered later and are also reported. Although these fields (in particular large-scale vertical velocity) have always been known to play a central role in atmospheric dynamics, they were never directly used since they were not measurable. The main result of our work is that these fields begin nowadays to enter the range of observability.

PACS 07.87.+v – Spaceborne and space research instruments, apparatus, and components (satellites, space vehicles, etc.).

PACS 95.75.Rs – Remote observing techniques.

PACS 84.40.Xb – Telemetry: remote control, remote sensing; radar.

PACS 92.70.Cp – Atmosphere.

1. – Introduction

It has been known since the beginning of modern scientific Meteorology (see the classical treatise by Richardson [1]) that, among the atmospheric fields, large-scale vertical velocity plays a central role in “weather” development and, consequently, its observation

^(*) The authors of this paper have agreed to not receive the proofs for correction.

could produce major improvements in forecast-analysis service operations. However, since this field was, and still is, not directly measurable, attention concerning its central dynamical role has, over the years, somewhat declined. As a consequence, papers concerning this topic are quite rare (a noticeable, recent exception is the paper of Muschinski *et al.* [2]). In fact, the main objective of our paper is to put forward the idea that the above variable is today entering the area of potential observability and, consequently, to propose some techniques that could make it possible to measure it from space.

The specific dynamical role of vertical velocity in synoptic-scale flows is most evident in the context of the quasi-geostrophic formulation [3] in which the evolution (time derivative) of the flow is determined by “residual” (first order in the “small” Rossby number) large-scale vertical velocities. In synoptic terms, every weather forecaster learns among the first notions that the atmosphere is strongly stratified with a stratification parameter (Coriolis parameter/Brunt-Väisälä frequency) of the order of 1/100. In practical terms, this entails that 1 cm/s of vertical velocity is “equivalent” to 1 m/s of horizontal velocity. In ordinary synoptic features (fronts, for example) large-scale vertical velocity is, however, of the order of a few centimeters per second and, as such, it is beyond the limits of detectability of the observational techniques discussed in this paper (in fact, of most available techniques!), even integrating the signal over vast portions of the atmosphere.

But vertical velocity plays also another central role in Meteorology: the advection of atmospheric water aloft. This process is very active in ordinary atmospheric convection that is, however, connected with vertical flows organized on “small” (of the order of kilometers) horizontal scales. Quite high vertical speeds (meters per second) can be developed in such processes that have been observed with radars from airplanes (for example from the ER-2 Doppler Radar, see Heymsfield [4]). But, due to the small scale, this type of observations cannot be presently used for the definition of vertical velocity at LAM scale.

Since the first applications of remote sensing to the observation of atmospheric water (see, for example, Browning and Collier [5]), it has become clear that other scales of aggregation are dynamically relevant. There are in fact motions that somehow synthesize the properties of synoptic-scale processes: wide precipitation bands, for example, which develop in extra-tropical cyclones and are characterized by synoptic horizontal scales (hundreds of kilometers) and speeds of the order of tens of centimeters per second. Although rich of precipitable water, these bands are, surprisingly, often stable with respect to ordinary convection in the vertical. The operating mechanism of water uplift is still unknown, but “mesoscale” (sub-synoptic, sub-frontal) vertical velocity must necessarily play a role in it. For this class of motions the observational techniques proposed in this paper are capable of producing useful measurements for both diagnostic and prognostic purposes at LAM scale. These “intermediate-scale” phenomena are particularly significant in the Mediterranean area, where the interaction of synoptic-scale perturbations with the complex-orography and land-sea structures generates a whole series of quite complex mesoscale features. It is to this class of motion that our attention has been specifically addressed in our effort of determining the measurability of large-scale vertical velocity in the atmosphere.

Although the specific meteorological phenomenology taken as target of the research reported here is that characterizing the Mediterranean region, many proposed notions and problems can be extended to other geographical areas. The LAMs used at present for weather forecasting in the Mediterranean area have horizontal resolutions approximately ranging from 30 km to 5 km and several tens of levels spanning the troposphere in the vertical. These models are run with initial and boundary conditions derived from global

forecasts and still suffer for the lack of adequate direct observations at regional scale. In our study particular attention has been paid to the measurement of large-scale vertical velocity, defined on the typical scale of a LAM-grid (10 km of horizontal resolution), using as target either condensed water or enhanced atmospheric turbulence. Since models of grid-size smaller than 30 km are capable of explicitly representing the subsynoptic-scale processes above referred to, the diagnostic and prognostic impact of such observations on LAM operations is, then, quite obvious. More complex is the problem of assessing the general impact of direct measurements of large-scale vertical velocity in the atmosphere on numerical weather forecast. In fact, the evaluation of such an impact critically depends on when, where and how⁽¹⁾ the measurements in question take place and what measure of skill is adopted. The problem is being analysed elsewhere and will be the object of other publications.

Monitoring the motion of condensed water is now possible with spaceborne weather radars. Investigations using such radars have been planned for more than 35 years (a review can be found in [6]), quite before the weight, size and cost limitations could be overcome thanks to advances in antenna technology, low-noise receivers and progress in electronics. The success of the Tropical Rainfall Measuring Mission [7] led to spaceborne weather radar being used as an instrument that is capable of observing the Earth's atmosphere on a global and long-term basis. In conjunction with the preparation of that mission, a first software code was developed by Meneghini [8] to evaluate the performance of the TRMM precipitation radar. It is here proposed to use a sophisticated radar system in the Ku band (13.78 GHz), which was developed for the Cassini mission, from the ISS altitude. This instrument presents a noteworthy flexibility so that it can be used in different programmable modes, changing the pulse length, the pulse repetition frequency and the pulse frequency, or even in the chirp mode, although the maximum peak transmitted power is limited to 70 W. The possibility of using the Cassini radar as a spaceborne weather radar onboard the International Space Station, has been simulated using a multifunctional software [9] called Spaceborne Weather Radar Simulator (SWRS).

Nevertheless, liquid water represents a tracer for the meteorological phenomena at an advanced stage of development. It would be interesting to obtain information on instabilities in their early stage, and observations of this kind may be performed through the monitoring of clear-air turbulence. Although a few instruments already exist on the ground for this purpose, these are characterized by large antennas and high transmitted power, and such characteristics have so far prevented their use from space. Furthermore, it should be noted that observations from space (*e.g.*, from 400 km altitude) of a beam-filling target, placed at a height of 4 km, requires a 40 dB gain in sensitivity with respect to ground-based observations (given the same antenna gain and pulse power). It is shown in sect. 5 that a spaceborne radar of this type is feasible, though at the limit of technological possibilities.

In this paper we discuss the general feasibility and the results obtainable adopting a particular sounding strategy for the measurements of light rain and clear-air turbulence fields from satellite-based radars. It is organized as follows: in sect. 2 a simplified version of the radar equation is proposed, while in sect. 3 the sounding strategy for vertical velocity measurements from space is presented. The performances of the satellite-based "cloud" and clear-air radar are respectively discussed in sects. 4 and 5.

⁽¹⁾ This difficulty is particularly evident in the case of "adaptive" approaches to observation: adjoint methods, etc.

2. – The weather radar equation

As stated above, the detection of large-scale instabilities in the atmosphere at an initial stage of their development is particularly important for forecasting major impact weather events. The spatial resolution in the measurements may be relatively poor with respect to the requirements of comparable missions, more oriented towards the micro-structure of precipitation. This has important consequences, since the vertical motion that has to be detected, although generally small, is coherent on relatively large scales, and can give a significant signal when integrated on a large volume. The microphysical radar targets within an incipient meso-structure could be either water drops in their early stage of growth or clear-air turbulence. Furthermore, in many practical LAM applications the vertical profile may be not as important as in other meteorological problems.

Under the above-defined conditions, assuming that the target homogeneously fills the antenna lobe, which has been supposed to be Gaussian, a simplified version of a signal-to-noise ratio (SNR) equation for a single pulse radar, is as follows:

$$(1) \quad \text{SNR} = P_t \cdot \frac{G^2 \cdot \vartheta_{3\text{dB}}^2 \cdot \lambda^2 \cdot c \cdot \tau^2}{2^{10} \cdot \pi^2 \cdot \ln 2 \cdot d^2 \cdot k \cdot T_a \cdot F} \cdot \eta,$$

where P_t is the transmitted power in Watt, G the antenna gain, τ the pulse length in seconds, $\vartheta_{3\text{dB}}$ the full 3dB antenna beamwidth in radians, d the distance from the radar to the target in meters, k the Boltzmann constant ($k = 1.38 \cdot 10^{-23} \text{ J}\cdot\text{K}^{-1}$), T_a the equivalent antenna noise temperature (assumed to be 290 K in the computations), and F the receiver noise figure. The quantity η is the radar reflectivity coefficient measured in m^{-1} and is due, respectively, to liquid water droplets or to clear-air turbulence.

The above equation is analyzed in sect. 4, to evaluate the performance of a “cloud” radar, and in sect. 5 to estimate the performances of a “clear-air” instrument.

3. – Sounding strategy for vertical velocity measurements

As already stated, the vertical profile of the atmospheric parameters of interest is not considered essential in the potential LAM applications in question here. Consequently, a vertical resolution of the order of 3000 m is considered acceptable. This corresponds to a pulse length τ of 20 μs (vertical sounding). The significant target may be found in the altitude range between 1000 m and 4000 m above sea level. In the following sections, two specific examples of radar are analyzed: the first operates at 13.78 GHz ($\approx 2 \text{ cm}$ wavelength), that is the frequency band of the TRMM instrument (we refer here to the re-use of the radar adopted in the Cassini mission); the second one has a wavelength of 23 cm and is more suitable for clear-air turbulence detection.

We have supposed that such radars are carried onboard the ISS, the velocity of which is approximately of $7 \text{ km}\cdot\text{s}^{-1}$. Assuming a 0.75° beamwidth, the Doppler effect at the border of the main lobe of the 2 cm wavelength radar results to be approximately $\pm 4209 \text{ Hz}$. For the 23 cm wavelength radar, a Doppler effect of $\pm 582 \text{ Hz}$ is found if a 1.1° beamwidth is assumed. These frequency values are significant, but do not represent a noteworthy spread of the spectrum if compared to the spectrum of the transmitted pulses.

The following sections show that a single-pulse sounding strategy does not assure sufficient values for the SNR (see eq. (1)). The low reflectivity values of cloud droplets or clear-air echoes cannot in fact be detected in this case using spaceborne radars with

“reasonable” technical parameters. Consequently, other techniques implying time integration must be used. However, the maximum integration time is limited by the satellite displacement. An “acceptable displacement” (10% of the field of view) defines a time-on-target of approximately 0.1 s (for a 400 km altitude satellite and a 1° beamwidth). The back-and-forward pulse flight time T_{bf} (from radar to target and back) is of the order of 2.6 ms. Assuming there are significant targets up to a height of 6 km at the most, the significant echo length would last 80 μ s. Such a time length includes meteorological, ground target and mirror echo. If the 20 μ s pulse length is also taken into account, the overall echo length results to be approximately 100 μ s.

Coherently with the above analysis, the following sounding strategy can be suggested: the transmitter is turned on for 2.6 ms and the receiver is then activated for the next 2.6 ms interval (50% of duty cycle). A series of 26 bursts of 100 μ s lengths are transmitted during transmission. Each burst is made up of five 20 μ s pulses at stepped frequencies (f_1 to f_5). The consequences of this sounding strategy, on both the SNR value and the vertical velocity detectability, are examined in the next two sections.

4. – The performance of a “cloud” radar

In this section, attention is focused on the use of the Cassini instrument since its flexibility offers the possibility of obtaining significant results. The SNR is evaluated in subsect. 4.1 for a single pulse using the Spaceborne Weather Radar Simulator (SWRS); in subsect. 4.2 the SNR is examined when the specific sounding strategy described in sect. 3 is adopted; finally, in subsect. 4.3, the feasibility of evaluating vertical velocity motions through phase measurements is dealt with.

The SWRS code [9] simulates reflected power from ground/sea and meteorological targets. It also provides an estimate of mirror image return. The SWRS input specifications can be modified to vary the antenna orientation, pulse duration, antenna radiation pattern, surface backscattering coefficient, vertical profile of reflectivity and pulse repetition frequency. In the framework of this study, it is specifically used to estimate the performances of the possible transformation of the Cassini radar into a space-borne weather radar.

4.1. *SNR for a single pulse.* – The target and instrument characteristics are the inputs to the simulator. The target characteristics comprise the vertical radar reflectivity (Z) profile and the radar back-scattering cross-section of the sea surface. In the example presented in this section, a stratiform vertical profile of rain and a rough sea state have been assumed. The vertical profile of reflectivity that has been used is a one-day average as observed by the *Albis* Swiss radar station on July 14, 1997 [10]: this is a typical stratiform profile, characterized by a bright band signature of a few hundred meters below the 0° C isotherm (maximum reflectivity equal to 27.7 dBZ) and a strong negative gradient above the melting layer (-9 dBZ·km⁻¹). As far as the sea-clutter model is concerned, the empirical model developed by Morchin [11] has been adopted. The relation between the radar reflectivity coefficient η (measured in m⁻¹) appearing in (1) and the radar reflectivity Z (measured in mm⁶·m⁻³) is

$$(2) \quad \eta = 10^{-18} \cdot \frac{\pi^5}{\lambda^4} \cdot |k|^2 \cdot Z,$$

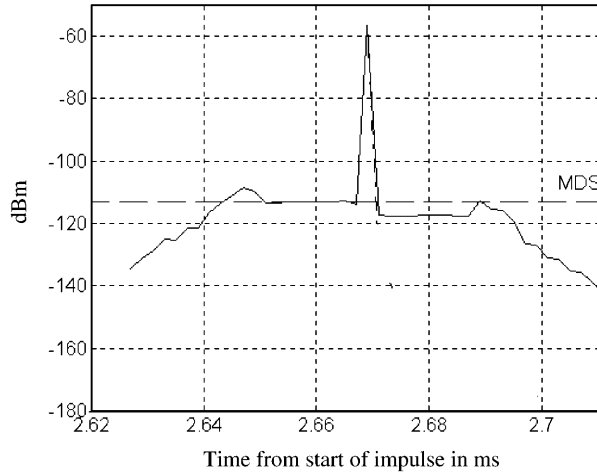


Fig. 1. – Example of received power (in dBm) obtainable with the SWRS simulator adopting the instrument characteristics described in subsect. 4'1.

where λ is measured in meters and $|k|^2 = \left| \frac{n^2 - 1}{n^2 + 2} \right|^2$; in our case $|k|^2$ is approximately 0.93 for liquid water droplets and 0.16 for ice (above the bright band).

Figure 1 shows the result of the simulation using the following instrument characteristics: $2 \mu\text{s}$ pulse length (300 m range resolution); the Cassini radar (operating at 13.78 GHz with a peak power of 70 W and a receiver noise figure of 3.5 dB) onboard a platform placed at an altitude of 400 km (*e.g.*, the ISS orbit) using a nadir pointing antenna with a 0.75° beamwidth (50.5 dB gain). It can be seen that the sea clutter contribution to the radar signal is received after the time T_{bf} equal to 2.67 ms. The signal received before the sea clutter contribution is due to the power backscattered from the meteorological target: a peak in the received power, which is caused by the bright band, is clearly detected at 2.65 ms. Since the meteorological targets taken into consideration in this paper are associated with light rain (less than 1 mm/h rain intensity), the power losses caused by attenuation have been neglected in the simulations. Experimental observations from meteorological satellites have shown the presence of a so-called “mirror” echo, almost symmetric to the surface return. The SWRS evaluates these effects by implementing the expression proposed by Meneghini and Atlas [12]. The output of this computation is visible in fig. 1 for t greater than 2.67 ms.

With the above-mentioned instrument characteristics, the SWRS-derived instrument sensitivity results to be 21.5 dBZ (limit case of $\text{SNR} = 1$). Obviously, a more restrictive condition than $\text{SNR} = 1$, *e.g.*, 90% probability of detection, would require an increased minimum detectable Z value (*e.g.*, +10 dB). If (1) and (2) are directly applied (with the same above-mentioned instrument characteristics), a minimum detectable Z , somewhat less than the one obtained through the simulation, is computed: for instance, 19.7 dBZ in correspondence to $\text{SNR} = 1$. The difference of 1.8 dB can easily be explained, since the true antenna diagram has been implemented in the simulator (that is, the simulator takes into account the detailed behaviour of the antenna pattern diagram as a function of the two azimuthal and zenithal angles, including secondary lobes). In what follows, given the “not-so-large” difference in the results, eq. (1) is systematically adopted to

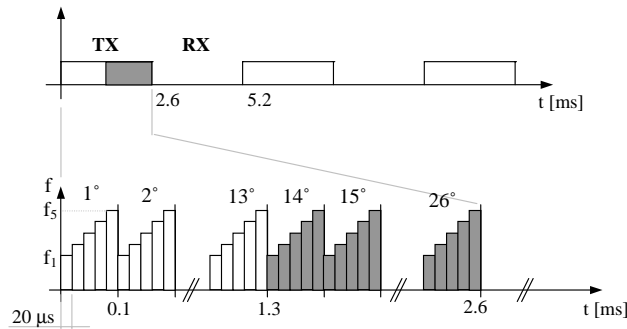


Fig. 2. – Schematic view of the sounding strategy proposed for cloud/rain detection and vertical velocity evaluation by cloud radar. For each 26-bursts train transmitted, two different samples could be generated after integration.

assess the order of magnitude of the minimum detectable signal, using various sounding strategies or different technical radar parameters.

4.2. Multiple pulses integration. – By using the sounding strategy suggested in sect. 3, the received signal may be integrated for the entire length of the reception, namely 2.6 ms. However, attention has to be paid to the specific characteristics of the received signal, especially as for what concerns its coherence. During each 100 μs burst, five different frequencies are in fact transmitted. Even if each of these were coherent with the others being derived from the same frequency source, the echoes would be completely uncorrelated in phase, being due to the sum of scattered signals from randomly distributed particles. Consequently, when integrating over each 100 μs burst, the SNR improvement is of the order $\sqrt{5}$ (approximately 3.5 dB) after frequency conversion. As far as the improvement due to the 26 burst trains is concerned, a completely different approach can be used. At least for half the 2.6 ms transmission time (13 burst trains), the scattering particles positions do not significantly change. Consequently, the signal may be assumed to be coherent, and the SNR improvement due to the coherent integration over 13 burst trains is of the order of 13 times (11 dB). Therefore, we could obtain two different integrated samples for vertical velocity evaluation (see next section) from the 26 burst train received; each of them is characterized by an SNR improvement approximately of 14.5 dB (a schematic view of the sounding strategy proposed for the weather radar is reported in fig. 2). A pulse length of 20 μs gives rise to another 20 dB improvement with respect to the 2 μs single-pulse case that was analysed in the previous section. In conclusion, the overall increase in the SNR is 34.5 dB; consequently, the minimum detectable Z becomes of the order of -14.8 dBZ.

The assumptions that have been made (homogeneous beam-filling, neglecting of noise increase by side-lobe spurious echoes, etc.) make this value only a “theoretical limit”. Nevertheless, the possibility of identifying liquid water particles generated in the early stage of the development of instability appears to be reasonably assured.

4.3. Large-scale vertical motion evaluations through phase shifts measurements. – Let us assume a vertical velocity of 1 ms^{-1} as target of the experiment. By adopting a technique that is similar to the one in use in standard meteorological radars, it is possible to compare the phase of the signal relative to the second half of the 26 burst trains with

the phase of the first 13 trains. In 1.3 ms, the vertical shift of the pattern of the scattering elements is of the order of 0.13 cm. This implies a phase shift of the order of 43° for a 13.78 GHz signal. At this point, it is necessary to evaluate whether this quantity is measurable, in comparison with other sources of phase shifts.

One source of error is evidently due to the fact that the radar target is slightly changed, due to the satellite motion itself, during the 1.3 ms time interval. The scattering volume has in fact changed in percentage by an amount equal to twice the ratio between the 9 m satellite shift and the antenna footprint, that is approximately 0.35%. Even though the contribution to the received signal of this term is in quadrature with the unchanged contribution, the phase error is less than 0.2° , which is much less than the phase shift that has to be measured.

Furthermore, since the meteorological sensor and its target are in relative motion to each other, the spectrum of the received radar echo is subject to a Doppler shift. For spaceborne weather radars, the relative velocity along the sensor-to-target line of sight is caused by satellite motion, Earth rotation and atmospheric target motion. Earth rotation causes Doppler shifts of almost two orders of magnitude lower than Doppler effects due to satellite motion (the only one here considered). As stated before, given the ISS orbital velocity of $7 \text{ km}\cdot\text{s}^{-1}$ and assuming an approximately 0.75° antenna lobe, the Doppler effect at the border of the main lobe itself is $\pm 4209 \text{ Hz}$. Due to the fact that the satellite moves during the 1.3 ms interval used for phase comparison, the various parts of the target itself will give contributions to the final echo with different Doppler values. In particular, the change in the Doppler effect can immediately be computed at the two extremes of the footprint, and is of the order of 14.5 Hz. Even if we assume such a change in the Doppler effect to be constant throughout the entire footprint, the total phase change in the signal during the given time interval is approximately 6.8° . This quantity is less than the quantity that has to be measured but can however be evaluated and taken care of through a specific correction algorithm.

In conclusion, the adoption of the sounding strategy suggested in sect. 3, permits a significant increase in the sensitivity of the instrument, and offers the possibility of detecting the instabilities in their “cloudy-stage” of formation. However, for the given Cassini KU-band radar, the presence of liquid water droplets is a necessary tracer of the considered phenomenon. Furthermore, phase shift measurements may allow the detection of large-scale coherent vertical motions, even in the presence of small vertical velocity components.

5. – The performance of a clear-air satellite-based radar

As stated in Introduction, the possibility of detecting meso-scale atmospheric instabilities at an initial stage of their developments (*i.e.* even before the cloud formation), is particularly important for forecasting purposes. This, of course, requires the measurement of atmospheric parameters in clear air using turbulence as a radar target. A few ground-based instruments already work to systematically measure clear-air turbulence echoes.

The significant technical parameters of some ground-based clear-air radars are reported in table I. The 2nd column refers to the Sousy MST radar located in Germany [13, 14]; the 3rd column refers to the Chatanika MST radar, originally located in Alaska and successively upgraded and transferred in Sondrestrom [13]; the 4th column refers to the Sunset MST radar located in Colorado [13, 15]; the last column refers to the Indian MST radar [14, 16, 17].

TABLE I. – *Technical parameters adopted by some ground-based radars, already working to systematically measure clear-air turbulence echoes.*

	Sousy MST radar	Chatanika MST radar	Sunset MST radar	Indian MST radar
Frequency	53.5 MHz	1.29 GHz	40.5 MHz	53 MHz
Peak power	0.6 MW	3.5 MW	0.125 MW	2.5 (0.18) ^(**) MW
Antenna Area Equivalent	3150 m ²	286 m ²	1800 m ²	3661 m ²
Antenna Gain	31 dB	48 dB	26 dB ^(*)	36 (32) ^(**) dB ^(*)
Antenna main lobe	5°	0.6°	9.8° ^(*)	3° (4.6°) ^(**)
Pulse length	up to 100 μs	up to 320 μs	6.7 μs	up to 32 μs
Pulse repetition frequency	0.4–80 kHz	100 Hz	6.25 kHz	62.5 Hz–8 kHz

(*) Computed on published data.

(**) The specifications in parentheses refer to ST-mode.

Interesting scattering echoes from clear-air turbulence have also been obtained through the use of profilers. Just as an example, let us remember the interesting data recently obtained in the Manus Island [18] through the use of an *S*-band profiler (2.835 GHz, 320 W peak power, 3.2° beamwidth) and an UHF profiler (915 MHz, 500 W peak power, 9° beamwidth). The observed turbulence events reported in that paper, of course, refer to meteorological events with stronger turbulence than that which is visible with the instruments listed in table I.

Let us imagine transposing one of the radars listed in table I from the ground to a satellite altitude of 400 km, with the specific aim of detecting from space the same weak turbulences at present detected from the ground. Even without considering the difficulties concerning the antenna physical dimensions and the transmitted power requirements, it would be necessary, as reported in the introduction, to have an instrument with an improved efficiency of approximately 40 dB.

In the following we will show that such a transposition is within the limits of present technology and can, in fact, be achieved. The present work, however, simply presents suggestions for future analysis and does not propose an optimized project. Our evaluations will therefore be made assuming the use of a 1.3 GHz radar (near the upper frequency that is useful for clear-air turbulence detection), in order not to deal with extremely large antennas.

5.1. Analytical considerations on turbulence. – The radar reflectivity coefficient η (which was introduced in sect. 2) is related to the turbulence structure constant C_n^2 (a parameter characterising the intensity of the atmospheric fluctuations, measured in m^{-2/3}) and to the wavelength λ , through the following equation [19]:

$$(3) \quad \eta = 0.38 \cdot C_n^2 \lambda^{-1/3} .$$

In turn, C_n^2 , as evaluated from radar observations, is related to the eddy dissipation rate ε (that is, a parameter which shows the energy dissipation rate inside the turbulence and is measured in m²s⁻³) by the equation (see [15])

$$(4) \quad \varepsilon = \gamma (C_n^2)^{3/2} \left(\frac{T}{P} \right)^3 ,$$

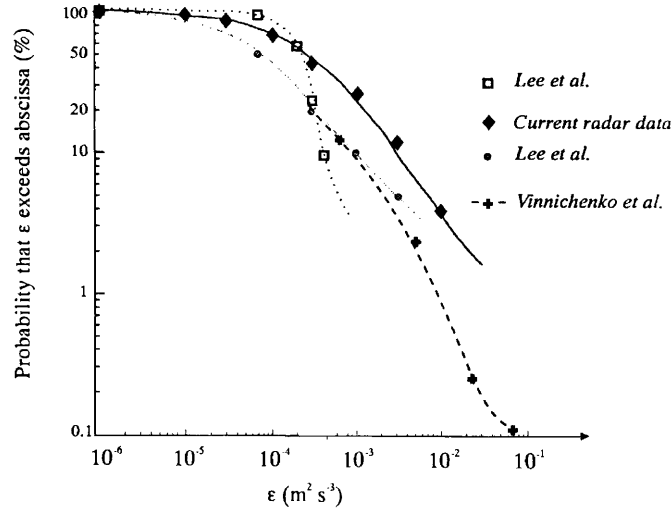


Fig. 3. – Examples of probability that a given eddy dissipation rate is exceeded in the troposphere (from [20]).

where T is the temperature in Kelvin and P is the pressure in mbar, while γ is a constant whose value is $1.14 \cdot 10^{22} \text{ m}^2 \cdot \text{mbar}^3 \cdot \text{K}^{-3} \cdot \text{s}^{-3}$ for the troposphere (without considering the presence of water vapor), or $3.43 \cdot 10^{21} \text{ m}^2 \cdot \text{mbar}^3 \cdot \text{K}^{-3} \cdot \text{s}^{-3}$ for the stratosphere.

In order to evaluate the percentage of times a given backscattered signal may be measured, it is important to know the probability for eddy dissipation rate to exceed a given value in the lower troposphere. For example, as reported in fig. 3, a value of $\varepsilon = 10^{-5} \text{ m}^2 \cdot \text{s}^{-3}$ is exceeded more than 90% of the times, while an eddy dissipation rate two orders of magnitude larger, *i.e.* $\varepsilon = 10^{-3} \text{ m}^2 \cdot \text{s}^{-3}$, is exceeded only, approximately, 20% of the times (see [20]).

In case of a nadir-looking spaceborne clear-air radar, the turbulence-induced backscattering at the assumed wavelength λ will be mainly due to spatial displacements of atmospheric irregularities Λ_B of approximately half of the wavelength (Bragg condition). In our case, being $\lambda = 23 \text{ cm}$, the characteristic length of the turbulence that can be measured would be $\Lambda_B \approx 11.5 \text{ cm}$, that is, a value well above the characteristic inner scale of tropospheric turbulence and, however, inside the typical inertial subrange of these turbulences.

The lifetime T_L of a turbulence depends on its characteristic length Λ_B and on its eddy dissipation rate ε , through the following expression (see [21]):

$$(5) \quad T_L = \Lambda^{2/3} \varepsilon^{-1/3}.$$

Hence, it is possible to plot the lifetime T_L as a function of the observational frequency f , for different values of eddy dissipation rates, as shown in fig. 4.

As far as the minimum usable wavelength for sounding is concerned, the following formula could be used [21]:

$$(6) \quad \Lambda_B = \frac{\lambda}{2} \geq \Lambda_{\text{lim}} = 5\pi \cdot \left(\frac{v^3}{\varepsilon} \right)^{1/4},$$

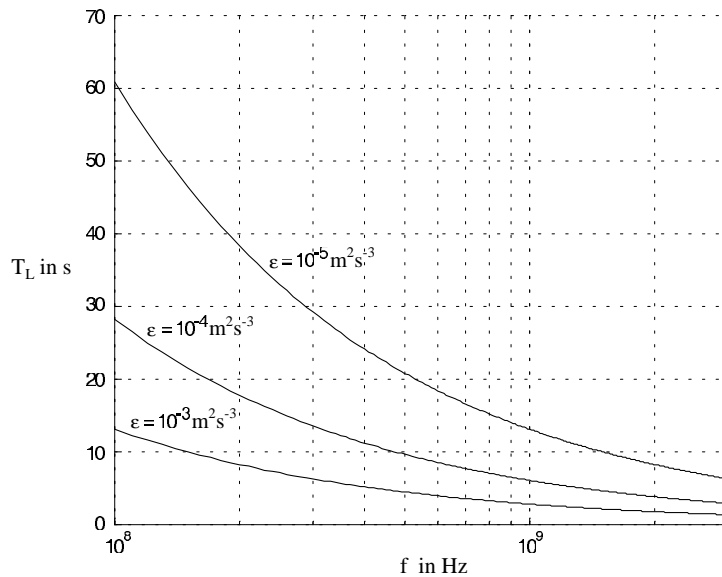


Fig. 4. – The lifetime T_L of turbulences in the troposphere as a function of the adopted sounding frequency f , for given values (expressed in m^2s^{-3}) of the eddy dissipation rate ε .

where ν is the kinematic viscosity (measured in m^2s^{-1}) and Λ_{lim} is the “limit” characteristic length of the turbulence that is considered acceptable as a radar target, namely 5π times the inner scale of the turbulence. Evaluating the kinematic viscosity ν as a function of standard temperature and density vertical profiles, the minimum usable wavelength as a function of height for given values of eddy dissipation rate is reported in fig. 5.

Finally, examples of measured vertical profiles of the structure constant C_n^2 , eddy dissipation rate ε and lifetime T_L are reported in fig. 6 (respectively, fig. 6a, 6b and 6c), together with an evaluation of the maximum frequency that can be used for sounding (fig. 6d). The C_n^2 profile was obtained from the Indian radar (see last column of table I) on June 17, 1994. The ε profile was obtained from C_n^2 using (4), while the T_L profile was obtained through the use of (5). The US Standard Atmosphere (1976) [23] was adopted for the profile of the eddy dissipation rate. The data presented in this figure should only be considered as order-of-magnitude-data, that are useful for the considerations that follow.

5.2. Characteristics of a clear-air L-band Satellite Radar. – Adopting a wavelength λ of 23 cm ($f = 1.3$ GHz), the radar signal may interact with turbulence with a lifetime T_L that is longer than a few seconds (see fig. 4). As fig. 5 shows, a radio frequency of 1.3 GHz may be used in sounding the troposphere to detect values of the eddy dissipation rates greater than $10^{-5} \text{ m}^2\text{s}^{-3}$. This is confirmed by the experimental results reported in fig. 6d, where the selected frequency is shown to be usable in the range from 4.5 km to 9 km.

As in the previous example of a weather radar (sect. 4), there is no specific interest in retrieving detailed vertical profiles. Consequently, “sufficiently long” duration pulses may be adopted (*e.g.*, 20 μs), which are compatible with the optimized sounding strategy proposed in sect. 3.

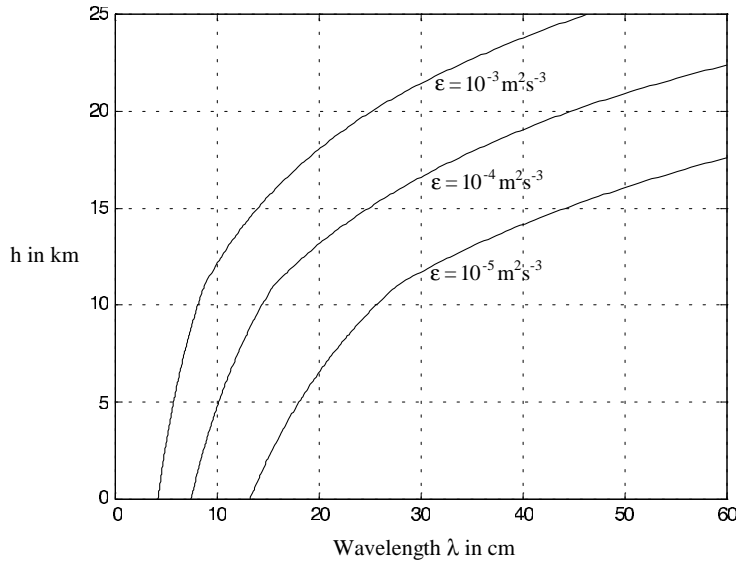


Fig. 5. – Minimum usable wavelength as a function of height, for given values (expressed in m^2s^{-3}) of the eddy dissipation rate ϵ .

In order to evaluate the feasibility of detecting enhanced clear-air turbulence from space, let us first evaluate the SNR using eqs. (1) and (3) for the Chatanika ground-based radar (see the parameters reported in table I, 3rd column). Assuming that the turbulence is placed at an altitude of 6500 m and it is characterised by a constant structure $C_n^2 = 7 \cdot 10^{-16} \text{ m}^{-2/3}$, the SNR for a single pulse results to be 32.1 dB. Let us now imagine to operate the radar onboard a satellite (at the ISS altitude), after modifying the transmitted power and the antenna characteristics. First of all, a transmitted 350 kW peak power (still a large amount for space applications; however we will discuss this point in the next subsection) will cause a 10 dB decrease in the SNR. Moreover, an antenna with a 1.1° beamwidth and a 44.3 dB gain, will cause a 2.4 dB decrease. Finally, the very different range causes a decrease in the SNR of 35.6 dB. In conclusion, for the “single pulse” operation mode, the loss in sensitivity of the satellite-based radar is approximately 48 dB (with respect to the Chatanika radar). This means a SNR of -16 dB for a turbulence characterised by a constant structure $C_n^2 = 7 \cdot 10^{-16} \text{ m}^{-2/3}$ and placed at an altitude of 6500 m.

The sounding strategy and the multiple pulse integration process proposed in sect. 3 however allows a 3.5 dB increase for each 100 μs burst, thanks to the non-coherent integration of five 20 μs pulses at different frequencies and a 14 dB increase due to the coherent integration of 26 burst trains over one cycle. Hence, for the same turbulence, an overall SNR equal to +1.5 dB may be reached.

In the present case it is also possible to extend the coherent integration over a longer period of time, say 166.4 ms (to assure a limited shift of the antenna footprint on the target), due to the longer lifetime of the turbulence. Consequently, a further SNR improvement of 12 dB may be obtained by integrating 16 non-adjacent cycles. Figure 7 shows a schematic view of the sounding strategy adopted in the preceding analysis.

As far as the possibility of measuring large-scale vertical motion by phase shifts is

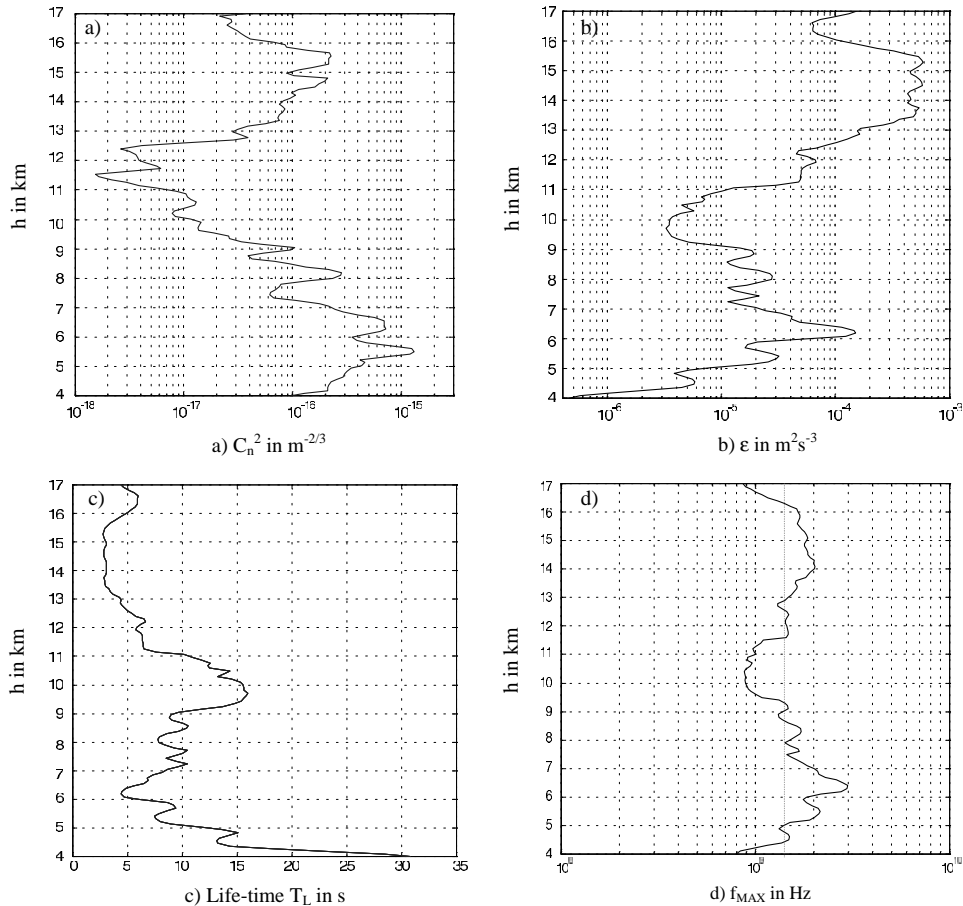


Fig. 6. – An example of a) measured C_n^2 profile (obtained on June 17, 1994 by the Indian MST radar) and the corresponding profiles of the b) eddy dissipation rate ε (see [22]), c) lifetime T_L and d) maximum usable f_{MAX} frequency for sounding, computed according to eq. (6). In the last figure the adopted frequency, which allows the detection of turbulences in the ranges between 4.5 km and 9 km or 13 km and 16.5 km, is also reported.

concerned, let us assume the same target characteristics of the experiment described in subsect. 4.3: a vertical velocity of 1 m/s. Consequently, the phase shift between cycles separated by 5.2 ms is approximately 8° . Here too, the same analysis performed in subsect. 4.3, *i.e.* the comparison with other sources of phase shifts, proves that these latter quantities are negligible, except for the phase shift due to the Doppler effect, which is estimated to be 10.5° , a quantity that can be taken care of using a specific correction algorithm.

5.3. Antenna dimensions and power limitations. – The antenna parameter that has been considered up to now is the gain (the beamwidth being strictly correlated to the gain itself), which is assumed to be 44.3 dB. To obtain such a parameter, a parabolic reflector with a diameter approximately equal to 14.5 m has to be used (assuming an aperture efficiency $\sigma = 0.7$), according to the following expression linking together the

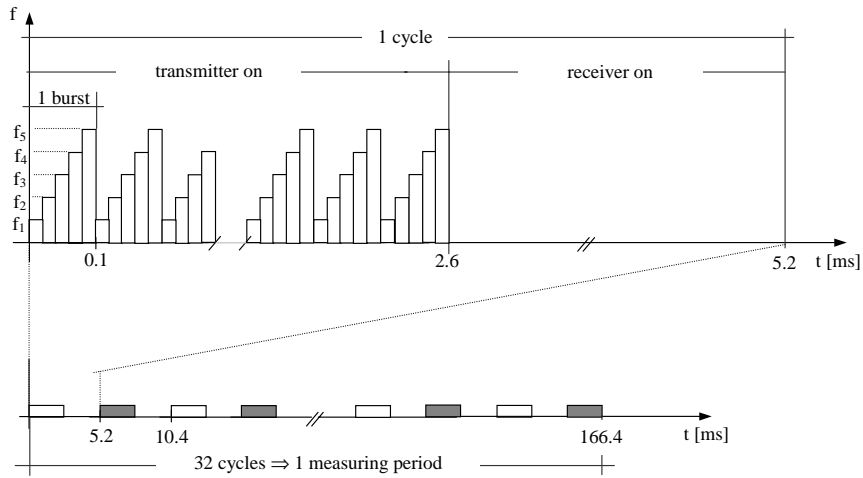


Fig. 7. – A schematic view of the sounding strategy proposed for the satellite-based clear-air radar, during a measuring period.

antenna gain G and its diameter d :

$$(7) \quad G = \sigma \left(\frac{\pi d}{\lambda} \right)^2 .$$

Obviously, such an antenna cannot be carried on board of any satellite.

Another approach could be represented by the use of an array antenna. Without going into technological details, attention can be focused on a two-dimensional broad-side radiating array uniformly fed, made up of 12×12 end-fire subarrays of dipoles (which radiate in increased directivity conditions). The required antenna parameters could be satisfied by assuming the positive interference of the radiation pattern of each end-fire

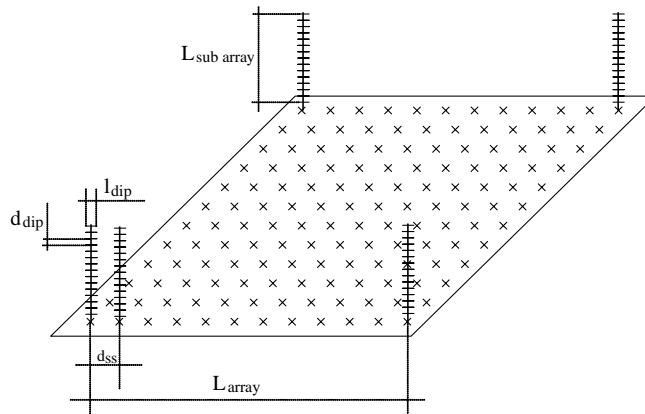


Fig. 8. – Sketch of the proposed antenna.

TABLE II. – *Characteristics of the antenna proposed for the clear-air satellite-based radar.*

n_{dip}	15	Numbers of dipoles for each subarray
l_{dip}	1λ (23 cm)	Length of dipoles
d_{dip}	0.75λ (17.3 cm)	Distance between dipoles
L_{subarray}	2.42 m	Subarray axial length
n_{ss}	12	Numbers of subarrays
d_{ss}	4λ (92.3 cm)	Distance between subarrays
L_{array}	10.15 m	Main array length (one side)
HPBW = $2 \cdot \vartheta_{3\text{dB}}$	1.058°	Half-power beamwidth
G_{max}	44.28 dB	Maximum gain
–13.15 dB ($\pm 1.7^\circ$)		First side lobe
–12.7 dB ($\pm 14.3^\circ$)		First grating lobe

subarray, which is obtainable when they are placed at more than one wavelength distance from each other. A 44.3 dB gain, for example, could be obtained placing these subarrays at a 4 wavelength distance from each other; each subarray is made up of 15 one-wavelength uniformly-fed dipoles, placed at a distance of 0.75λ from each other. The main characteristics of such an antenna are reported in table II, while its sketch is shown in fig. 8. Through a specific synthesis procedure of this antenna, and adopting a non-uniform displacement and feed of the active elements, is however possible to improve the radiation pattern, especially as far as the reduction of the first secondary lobes and the first grating lobes levels is concerned. In the example examined they are placed, respectively, at $\pm 1.7^\circ$ and $\pm 14.3^\circ$ from the nadir-looking direction. Although their levels (respectively of -13.2 dB and -12.7 dB from the main lobe level) are not so critical, maybe they can cause some problems in the measurement, in particular if stronger turbulences are placed in those directions. In fact, even if the main echo is obtained from the nadir-looking direction, for example from a turbulence placed at 6.5 km altitude, the echoes deriving from the other “critical” directions come from the presence of other instabilities placed at altitudes, respectively, of ≈ 6.5 km and ≈ 7 km, and displaced from the previous one of ≈ 12 km and ≈ 100 km. If these turbulences are stronger than that filling the main lobe, they could bring to a “dangerous” overestimation on the measurement.

Finally, as far as the required power request is concerned, the proposed peak power of 350 kW seems to be much higher for space application than can reasonably be acceptable. A specific atmospheric sampling procedure could be adopted: sampling the atmosphere just once every 10 s (namely one sample every 70 km). In this way the energy required for the transmission of the 32 cycles (4160 pulses) present in one measuring period, that is equal to the product between the number of transmitted pulses, the pulse length and the peak power, is approximately 29120 J. As a consequence, the mean transmitted power with the assumed sounding strategy, is approximately equal to 3 kW. The required power supply is therefore within the realm of technical possibilities, even if the presence of an energy accumulator is however unavoidable (let us remember that the energy accumulated in a car battery is of the order of $2 \cdot 10^6$ J).

These order-of-magnitude evaluations obviously do not define an optimised design of a clear-air radar operating from space; rather they were derived to show the feasibility of such an instrument.

6. – Conclusions

Numerical Weather Forecast models, in particular Limited Area Models for meteorological analysis-forecast at regional scale, nowadays suffer for the lack of adequate observations input at least as much as the definition of sub-grid dynamics.

As remarked in Introduction, the central dynamical role of large-scale vertical velocity has been well known since the time of the first development of the equations of motion for atmospheric flow [1].

However, since their direct measurements proposed insurmountable problems, these have been considered only as diagnostic (derived *a posteriori* from measurable fields) rather than prognostic (directly used in the forecast process) variables. Vertical velocity in ordinary synoptic processes (for example, frontal dynamics) is still too small for direct measurement.

There are motions, however, that somehow synthesize the properties of synoptic-scale and small-scale processes: wide precipitation bands, for example, that are characterized by synoptic horizontal scales (hundreds of kilometers) and speeds of the order of tens of centimeters per second. For this class of motions, the observational techniques proposed in this paper are capable of producing useful measurements both for diagnostic and prognostic purposes at LAM scale. This kind of motions is the ideal target of our study.

Specific quantitative estimate of the “impact” of observations of the type proposed on LAM analysis and prediction requires specific analysis that is under way. The results will be the object of future publications.

In this paper we propose a particular sounding strategy for the measurement from space of large-scale vertical velocity and other important meteorological fields, like rain and clear-air turbulence. In fact, this strategy could allow the evaluation of air instabilities at the first stage of their development (turbulences) and at a developed stage (drizzle and “light” rain) with a sufficient SNR, operating respectively with a clear-air radar and a rain radar, carried on board a satellite. Through phase measurements is then possible to obtain important information on vertical velocity, providing evidence that the above variables are nowadays entering the area of potential observability.

* * *

This work has been funded by the grants ASI I/R/67/00 and ASI I/R/102/01.

REFERENCES

- [1] RICHARDSON L. F., *Weather Prediction by Numerical Processes* (Cambridge University Press) 1922.
- [2] MUSCHINSKI A., CHILSON P. B., KERN S., NIELINGER J., SCHMIDT G. and PRENOSIL T., *J. Atmos. Sci.*, **56** (1990) 1248.
- [3] CHARNEY J. G., *J. Meteorol.*, **6** (1949) 371.
- [4] HEYMSFIELD G. H., *J. Atmos. Ocean. Tech.*, **13** (1996) 795.
- [5] BROWNING K. A. and COLLIER C. G., *Rev. Geophys.*, **27** (1989) 345.
- [6] MENEGHINI R. and KOZU T., *Spaceborne Weather Radar* (Artech House) 1990.
- [7] KUMMEROW C., BARNES W., KOZU T., SHIUE J. and SIMPSON J., *J. Atmos. Ocean. Technol.*, **15** (1998) 809.
- [8] MENEGHINI R., *Analysis of Radar and Radar-Radiometer Methods for Spaceborne Measurements of Precipitation*, submitted to the Graduate School of Engineering in partial fulfillment of the requirements for the degree of Doctor of Philosophy at Kyoto University (1995).

- [9] PAVONE S., ZOCCALI I., GABELLA M. and PERONA G., *Phys. Chem. Earth*, **25** (2000) 883.
- [10] GERMANN U., *Estimating the local vertical reflectivity profile for precipitation for extrapolation*, paper presented at the *COST-75 Final International Seminar on Advanced Weather Radar Systems*, edited by G. C. COLLIER, the Commission of the European Communities, EUR 18567 EN (Locarno, Switzerland) 1999, pp. 485-492.
- [11] MORCHIN W. C., *Airborne Early Warning Radar* (Artech House) 1990.
- [12] MENEGHINI R. and ATLAS D., *J. Atmos. Ocean. Technol.*, **2** (1985) 400.
- [13] BALSLEY B. B., *J. Atmos. Terr. Phys.*, **43** (1981) 495.
- [14] HOCKING W. K., *Radio Sci.*, **32** (1997) 2241.
- [15] GAGE K. S., GREEN J. L. and VANZANDT T. E., *Radio Sci.*, **15** (1980) 407.
- [16] JAIN A. R., JAYA RAO Y., RAO P. B., ANANDAN V. K., DAMLE S. H., BARAMURALIDHAR P., KULAKARNI A. and VISWANATHAN G., *Radio Sci.*, **30** (1995) 1139.
- [17] PATRA A. K., ANANDAN V. K., RAO P. B. and JAIN A. R., *Radio Sci.*, **30** (1995) 1159.
- [18] WILLIAMS C. R., ECKLUND W. L., JOHNSTON P. E. and GAGE K. S., *J. Atmos. Ocean. Technol.*, **17** (2000) 949.
- [19] GOSSARD E. E. and STRAUCH R. G., *Radar Observation of Clear-Air and Clouds* (Elsevier) 1983.
- [20] HOCKING W. K. and MU P. K. L., *J. Atmos. Solar-Terr. Phys.*, **59** (1997) 1779.
- [21] TATARSKII V. I., *Wave Propagation in a Turbulent Medium* (McGraw-Hill) 1971.
- [22] NARAYANA RAO D., KISHORE P., NARAYANA RAO T., VIJAYA BHASKARA RAO S., KRISHNA REDDY K., YARRAIAH M. and HAREESH M., *Radio Sci.*, **32** (1997) 1375.
- [23] JURSA A. S., *Handbook of geophysical and the space environment*, Air Force Geophysical Laboratory, U.S. Air Force (1985).